Journal of Solid State Chemistry 182 (2009) 1164–1170

Contents lists available at ScienceDirect

Journal of Solid State Chemistry

journal homepage: www.elsevier.com/locate/jssc

Synthesis and magnetic properties of rare earth ruthenates, $Ln_5Ru_2O_{12}$ (Ln = Pr, Nd, Sm–Tb)

M. Bharathy [a], W.R. Gemmill [a], A.H. Fox [a], J. Darriet [b], M.D. Smith [a], J. Hadermann [c], M.S. Remy [a], H.-C. zur Loye [a,*]

[a] Department of Chemistry and Biochemistry, University of South Carolina, Columbia, SC 29208, USA
[b] Institut de Chimie de la Matière Condensée de Bordeaux (C.N.R.S), Bordeaux, France
[c] University of Antwerp, Belgium

ARTICLE INFO

Article history:
Received 9 November 2008
Received in revised form
7 January 2009
Accepted 6 February 2009
Available online 21 February 2009

Keywords:
$Ln_5M_2O_{12}$
TEM
Hydroxide fluxes
Twinned crystals
Metal–metal bonding

ABSTRACT

Single crystals of $Ln_5Ru_2O_{12}$ (Ln = Pr, Nd, Sm–Tb) were grown out of either NaOH or KOH fluxes in sealed silver tubes. The crystals of all the phases were observed to be twinned as confirmed by TEM studies. The series crystallize in the $C2/m$ monoclinic system with lattice parameters, a = 12.4049(4)–12.7621(6) Å, b = 5.8414(2)–5.9488(3) Å, c = 7.3489(2)–7.6424(4) Å, β = 107.425(3)–107.432(2)° and Z = 2. The crystal structure is isotypic with the defect/disorder model of $Ln_5Re_2O_{12}$ (Ln = Y, Gd) and consists of one dimensional edge shared RuO_6 octahedral chains separated by a two dimensional LnO_x polyhedral framework. Magnetic measurements indicate paramagnetic and antiferromagnetic behavior for Ln = Nd, Sm–Gd and Ln = Tb, respectively.

1. Introduction

Low dimensional transition metal containing oxides are of interest for their electronic [1,2] and magnetic properties [3–8]. Unusual electronic phenomena, such as spin-Peierls instability, and spin-holon separation have been observed in oxides such as $GeCuO_3^1$, and $SrCuO_2^2$ while low dimensional magnetism has been observed in Ln_3MO_7 (Ln = La, Pr, Nd, Sm, Eu; M = Mo, Ru, Os, Ir) [3–6] and $Ln_5M_2O_{12}$ (Ln = Y, Gd; M = Mo, Re) [7–9]. The magnetic phenomenon in the $Ln_5M_2O_{12}$ series is particularly interesting due to the presence of two magnetically active components in the structure, the rare earth ion and the M_2O_{10} dimers. The alternating short and long metal-to-metal distances are thought to be indicative of some degree of metal–metal bonding, which allows for one unpaired electron per M_2 dimer due to the average oxidation state of +4.5 for M [7–9]. The magnetic contribution of the M_2O_{10} dimers is usually masked by the much larger moments of the rare earth ions (Ln = Tb and Ho) [7], but its distinct contribution is observed in the presence of nonmagnetic ions (e.g. Ln = Y) [8].

An interesting transition metal substitution in the $Ln_5M_2O_{12}$ series worth pursuing is that of ruthenium, since it can take up variable oxidation states and has the appropriate size to occupy the M position. Oxides containing ruthenium in its most stable +5 oxidation state have been routinely prepared by the solid-state method at high reaction temperatures (>900 °C) [10,11]. An alternative approach is the use of highly oxidizing molten hydroxide fluxes, which lower the reaction temperatures while acting as solvent media for the starting oxides. This approach has been used successfully for the preparation of oxides such as Sr_3LiRuO_6 [12] and $Ln_{14}Na_3Ru_6O_{36}$ (Ln = Pr, Nd) [13], containing ruthenium in the +5 oxidation state. Using the same approach we recently isolated the series $Ln_5Ru_2O_{12}$ (Ln = Pr, Nd, Sm–Tb) (where the average oxidation state of ruthenium is +4.5) from either NaOH or KOH fluxes in sealed silver tubes. Herein we report the crystal growth, structural and magnetic characterization of the series $Ln_5Ru_2O_{12}$ (Ln = Pr, Nd, Sm–Tb).

2. Experimental section

2.1. Materials

The lanthanide oxides, Ln_2O_3 (Alfa Aesar, REaction, 99.9%), were fired at 1000 °C for 12 h prior to use in the reactions. Ru powder (Engelhard, 99.5%), NaOH (Fisher, ACS reagent), and KOH (Fisher, ACS reagent) were used as received. RuO_2 was prepared by heating Ru powder at 1050 °C in air for 24 h.

* Corresponding author. Fax: +1 803 777 8508.
E-mail address: zurloye@mail.chem.sc.edu (H.-C. zur Loye).

0022-4596/$ - see front matter © 2009 Elsevier Inc. All rights reserved.
doi:10.1016/j.jssc.2009.02.013

2.2. Crystal growth

Single crystals of $Ln_5Ru_2O_{12}$ (Ln = Sm–Tb) were grown out of NaOH flux (10 mmol) using 1 mmol each of Ln_2O_3 and Ru powder and one gram of water. $Pr_5Ru_2O_{12}$ and $Nd_5Ru_2O_{12}$ were obtained from a KOH flux (7 mmol) and RuO_2 (1 mmol). The reaction mixtures contained in sealed silver tubes were heated at 600 °C for 12 h and cooled to 500 °C at the rate of 1 °C/min, followed by turning off the furnace. Black crystals of each phase were separated from the flux by washing with water, aided by sonication. Attempts to obtain quality crystals of $Nd_5Ru_2O_{12}$ for diffraction were unsuccessful. Reactions performed in silver crucibles did not yield the desired products and the product obtained was found to be sensitive to the water content and the hydroxide flux employed for synthesis. For larger rare earth substitutions, (Ln = Pr, Nd), the use of both NaOH and KOH also resulted in the formation of other oxides, $Ln_{14}A_3Ru_6O_{36}$ (A = Na,^{13}K) (with Na/K being incorporated into the structure) as a secondary phase.

2.3. SEM and HRTEM

Environmental scanning electron micrographs (ESEM) of the single crystals were obtained using a FEI Quanta 200 ESEM instrument utilized in the low vacuum mode. ESEM images of representative crystals of $Sm_5Ru_2O_{12}$ and $Tb_5Ru_2O_{12}$ are shown in Fig. 1a and b, respectively. Energy dispersive spectroscopy (EDS) verified the presence of the rare earth element (neodymium, samarium, europium, gadolinium, and terbium) and ruthenium for $Ln_5Ru_2O_{12}$ (Ln = Pr, Nd, Sm–Tb). Furthermore, within the detection limit of the instrument, no other extraneous elements were detected. High resolution TEM images were taken on a Jeol 4000EX microscope. Simulations of high resolution microscopy images were carried out using the MacTempas software suite.

2.4. Single crystal X-ray diffraction

X-ray diffraction intensity measurements of small black crystals were performed using Bruker Nonius Kappa CCD and Bruker SMART APEX CCD-based diffractometers using sealed tube graphite monochromated Mo$K\alpha$ radiation. Data were reduced using the specific software packages supplied with the diffractometers. An absorption correction was applied using the Gaussian method (for data collected on Bruker Nonius Kappa CCD) and SADABS [14] in the software suite of SMART (for data collected on Bruker SMART APEX CCD). The structures were solved using direct methods of SHELXS97 [15] and refined using either JANA2000 [16] or SHELXL97 [17]. The twin laws were identified using GEMINI [18] (For Ln = Gd and Eu) and the TwinRotMat program implemented in PLATON [19] suite (For Ln = Pr). Relevant crystallographic data for $Ln_5Ru_2O_{12}$ (Ln = Pr, Eu–Tb) are compiled in Table 1. The atomic positions and selected bond distances are summarized in Tables 2 and 3, respectively.

2.5. Magnetic susceptibility

Magnetic susceptibility of the series $Ln_5Ru_2O_{12}$ (Ln = Nd, Sm–Tb) was measured using a Quantum Design MPMS XL SQUID magnetometer. For the magnetic measurements, loose crystals of $Ln_5Ru_2O_{12}$ (Ln = Nd, Sm–Tb) were placed into gelatin capsules, which were in turn placed inside plastic straws. Samples were measured under both zero-field-cooled (ZFC) and field-cooled (FC) conditions. For all measurements, the magnetization was measured in the temperature range of 2–300 K. Susceptibility measurements were carried out in applied fields of 1 or 10 kG. The very small diamagnetic contribution of the gelatin capsule containing the sample had a negligible contribution to the overall magnetization, which was dominated by the sample signal.

3. Results and discussion

3.1. Crystal structures

The crystals of $Ln_5Ru_2O_{12}$ (Ln = Pr, Sm–Gd) were mostly twinned as already observed in the analogous $Ln_5Re_2O_{12}$ oxides [8,18–20]. The twin fractions appeared to be related either by a two-fold rotation around the reciprocal [20$\bar{1}$] axis

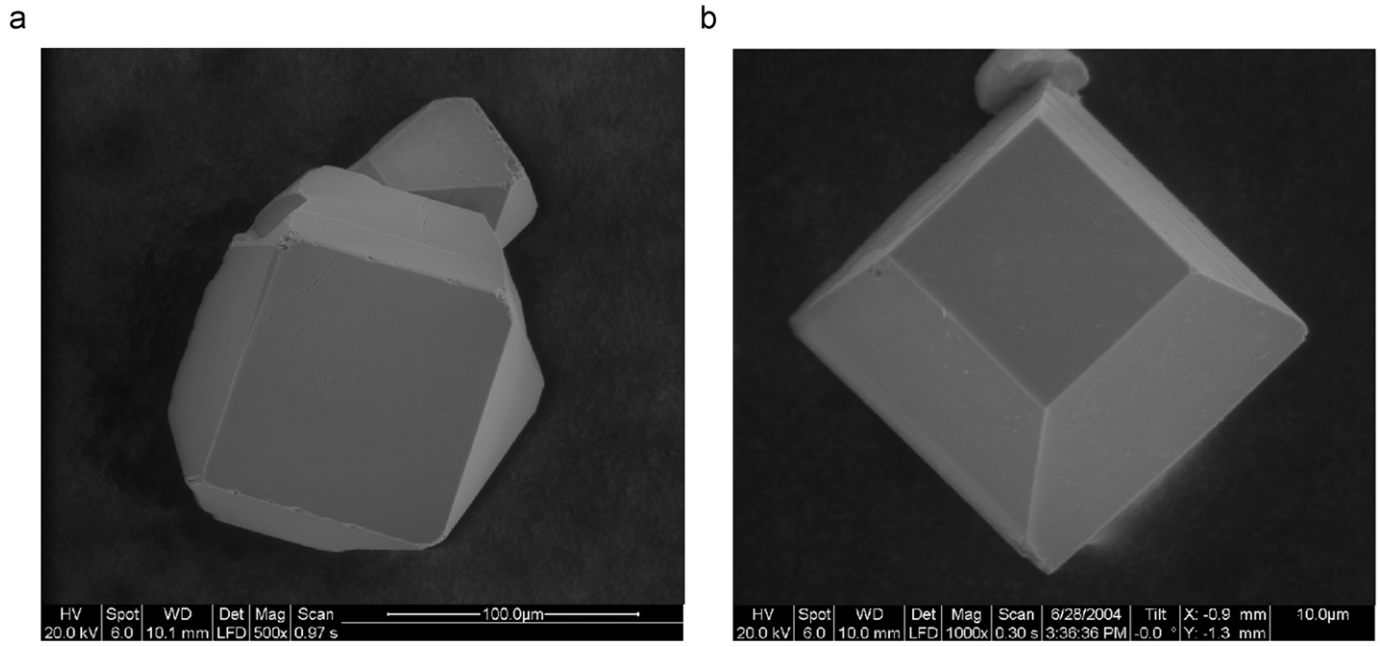

Fig. 1. SEM images of representative single crystals of: (a) $Sm_5Ru_2O_{12}$ and (b) $Tb_5Ru_2O_{12}$.

Table 1
Crystal data and structure refinement details for $Ln_5Ru_2O_{12}$ (Ln = Pr, Eu, Gd, Tb[a]).

Empirical formula	$Pr_5Ru_2O_{12}$	$Eu_5Ru_2O_{12}$	$Gd_5Ru_2O_{12}$	$Tb_5Ru_2O_{12}$[a]
Crystal habit, color	Rod, black	Rod, black	Tablet, black	Fragment, black
Crystal size (mm^3)	$0.08 \times 0.05 \times 0.03$	$0.02 \times 0.03 \times 0.08$	$0.02 \times 0.04 \times 0.08$	$0.06 \times 0.08 \times 0.12$
Crystal system	Monoclinic	Monoclinic	Monoclinic	Monoclinic
Formula weight (g/mol)	1098.69	1153.94	1180.39	1188.74
Space group	$C2/m$	$C2/m$	$C2/m$	$C2/m$
Unit cell dimensions				
a (Å)	12.7621(6)	12.5111(8)	12.4618(10)	12.4049(4)
b (Å)	5.9488(3)	5.8712(4)	5.8578(5)	5.8414(2)
c (Å)	7.6424(4)	7.4468(4)	7.4135(6)	7.3489(2)
β (°)	107.416(1)	107.432(2)	107.425(3)	107.363(1)
V ($Å^3$)	553.61(5)	521.88(6)	516.34(7)	508.25(3)
Z	2	2	2	2
Density (calculated) (mg/m^3)	6.591	7.343	7.592	7.768
$F(000)$	958	998	1008	1018
θ_{max} (deg)	35.642	32.61	32.56	39.99
Recording reciprocal space	$-20 \leqslant h \leqslant 20$, $-9 \leqslant k \leqslant 9$, $-12 \leqslant l \leqslant 12$	$-18 \leqslant h \leqslant 18$, $-8 \leqslant k \leqslant 8$, $-11 \leqslant l \leqslant 11$	$-18 \leqslant h \leqslant 18$, $-8 \leqslant k \leqslant 8$, $-11 \leqslant l \leqslant 11$	$-20 \leqslant h \leqslant 18$, $-9 \leqslant k \leqslant 9$, $-11 \leqslant l \leqslant 11$
μ ($mm^{-1)}$	24.266	32.448	34.539	37.253
No. of reflections	1380	3682	3117	5623
Refinement	F^2	F^2	F^2	F^2
No. of variables	54	50	64	62
Independent reflections	1380 ($R_{int} = 0.0340$)	3682 ($R_{int} = 0.0000$)	3117 ($R_{int} = 0.0000$)	1216 ($R_{int} = 0.0293$)
GoF	1.061	1.135	1.049	1.299
R indices [$I > 2$sigma(I)]	$R1 = 0.0276$, w$R2 = 0.0617$	$R1 = 0.0376$, w$R2 = 0.0974$	$R1 = 0.0394$, w$R2 = 0.0995$	$R1 = 0.0252$, w$R2 = 0.0524$
Max/min $\Delta\rho$ ($e^-/Å^3$)	3.765 and −4.557	4.577 and −5.429	5.478 and −4.709	1.879 and −2.031

[a] Refinement carried out neglecting the minor twin lattice.

Table 2
Atomic coordinates and equivalent isotropic displacement parameters for $Ln_5Ru_2O_{12}$ (Ln = Pr, Eu, Gd, Tb).

	x	y	z	U(eq) ($Å^2$)	Occupancy
$Pr_5Ru_2O_{12}$					
Ru(1)	0	0.23567(9)	0	0.00540(11)	1
Pr(1)	0.30740(4)	0	0.64219(9)	0.00590(10)	1
Pr(2)	0.30950(4)	0	0.16665(9)	0.00672(11)	1
Pr(3)	0	0	0.5000	0.00662(11)	1
O(1)	0.1587(3)	0.2545(7)	0.0781(9)	0.0082(7)	1
O(2)	0.3458(3)	0.2510(7)	0.4218(9)	0.0076(7)	1
O(3)	0.5006(7)	0	0.1716(8)	0.0076(9)	1
O(4)	0.0008(7)	0	0.1842(8)	0.0102(10)	1
$Eu_5Ru_2O_{12}$					
Ru(1)	0	0.23676(19)	0	0.0029(2)	0.956(4)
Eu(1)	0.30904(6)	0	0.1666(10)	0.0042(2)	1
Eu(2)	0.30470(6)	0	0.64269(10)	0.0037(2)	1
Eu(3)	0	0	0.5000	0.0049(2)	0.956(4)
O(1)	0.3432(6)	0.2495(15)	0.4243(9)	0.0059(13)	1
O(2)	0.1611(6)	0.2565(14)	0.0792(9)	0.0049(12)	1
O(3)	−0.0008(10)	0	0.8116(16)	0.008(2)	0.956(4)
O(4)	0.0013(9)	0.5000	0.1777(15)	0.004(2)	0.956(4)
Ru(1A)	0	0.237(5)	0.5000	0.009(6)	0.044(4)
Eu(3A)	0	0	0	0.007(6)	0.044(4)
O(3A)	0.010(2)	0	0.3110(16)	0.010	0.044(4)
O(4A)	0.040(2)	0.5000	0.679(11)	0.010	0.044(4)
$Gd_5Ru_2O_{12}$					
Ru(1)	0	0.2368(3)	0	0.0031(3)	0.951(6)
Gd(1)	0.30909(8)	0	0.16729(14)	0.0047(3)	1
Gd(2)	0.30436(8)	0	0.64216(14)	0.0044(3)	1
Gd(3)	0	0	0.5000	0.0051(3)	0.951(6)
O(1)	0.3416(9)	0.249 (2)	0.4247(14)	0.0069(19)	1
O(2)	0.1623(9)	0.256(2)	0.0800(14)	0.0067(18)	1
O(3)	−0.0007(14)	0	0.809(2)	0.008(3)	0.951(6)
O(4)	0.0003(13)	0.5000	0.179(2)	0.003(3)	0.951(6)
Ru(1A)	0	0.239(7)	0.5000	0.014(8)	0.049(6)
Gd(3A)	0	0	0	0.014(8)	0.049(6)
O(3A)	0.07 (3)	0	0.38 (4)	0.015	0.049(6)

Table 2 (*continued*)

	x	*y*	*z*	*U*(eq) (Å^2)	Occupancy
O(4A)	−0.01 (3)	0.5	0.70 (5)	0.015	0.049(6)
$Tb_5Ru_2O_{12}$					
Ru(1)	0	0.23766(9)	0	0.00520(11)	0.9767(17)
Tb(1)	0.30867(3)	0	0.16724(4)	0.00643(9)	1
Tb(2)	0.30357(3)	0	0.64172(4)	0.00595(8)	1
Tb(3)	0	0	0.5	0.00751(10)	0.95
O(1)	0.3472(3)	0.2500 (6)	0.4249(5)	0.0069(6)	1
O(2)	0.1625(3)	0.2578(6)	0.0816(5)	0.0069(6)	1
O(3)	−0.0004(5)	0	0.8105(7)	0.096(9)	0.9767(17)
O(4)	0.0003(4)	0.5	0.1822(7)	0.0088(9)	0.9767(17)
Ru(1A)	0	0.238(5)	0.5	0.015(5)	0.0233(17)
Tb(3A)	0	0	0	0.016(5)	0.0233(17)
Tb(3B)	0	0.5	0.5	0.005(4)	0.0233(17)
O(3A)	−0.01(2)	0	0.303(11)	0.015	0.0233(17)
O(4A)	0.02(2)	0.5	0.684(7)	0.015	0.0233(17)

Table 3
Selected bond distances (Å) for $Ln_5Ru_2O_{12}$ (*Ln* = Pr, Eu, Gd, Tb).

	$Pr_5Ru_2O_{12}$	$Eu_5Ru_2O_{12}$
Ln(1)–O(1) (× 2)	2.517(6)	2.349(8)
Ln(1)–O(2) (× 2)	2.408(6)	2.323(8)
Ln(1)–O(2) (× 2)	2.384(4)	2.438(7)
Ln(1)–O(3) (× 1)	2.438(8)	
Ln(2)–O(1) (× 2)	2.382(4)	2.299(8)
Ln(2)–O(1) (× 2)	2.500(6)	2.344(8)
Ln(2)–O(2) (× 2)	2.392(4)	2.446(7)
Ln(2)–O(4)	2.417(6)	2.395(11)
Ln(3)–O(1) (× 4)	2.389(12)	2.380(8)
Ln(3)–O(3) (× 2)	2.296(16)	2.324(12)
Ru–O(1) (× 2)	1.936(4)	1.927(7)
Ru–O(3) (× 2)	1.984(4)	1.973(8)
Ru–O(4) (× 2)	2.046(3)	2.031(7)
Ru–Ru (short)	2.8038(11)	2.780(2)
Ru–Ru (long)	3.1450(11)	3.091(2)
	$Gd_5Ru_2O_{12}$	$Tb_5Ru_2O_{12}$
Ln(1)–O(1) (× 2)	2.339(11)	2.325(3)
Ln(1)–O(2) (× 2)	2.302(11)	2.296(3)
Ln(1)–O(2) (× 2)	2.434(10)	2.422(3)
Ln(2)–O(1) (× 2)	2.275(12)	2.307(3)
Ln(2)–O(1) (× 2)	2.322(11)	2.341(3)
Ln(2)–O(2) (× 2)	2.439(11)	2.409(3)
Ln(2)–O(4)	2.397(15)	2.391(5)
Ln(3)–O(1) (× 4)	2.389(12)	2.325(3)
Ln(3)–O(3) (× 2)	2.296(16)	2.283(5)
Ru–O(2) (× 2)	1.933(11)	1.928(3)
Ru–O(3) (× 2)	1.979(11)	1.966(4)
Ru–O(4) (× 2)	2.036(9)	2.035(3)
Ru–Ru (short)	2.774(3)	2.7765(11)
Ru–Ru (long)	3.084(3)	3.0649(11)

(*Ln* = Pr, Eu, Gd), or by a mirror parallel to the plane (100) and a translation of $\frac{1}{2}$ along the *b* axis (*Ln* = Sm, Eu, Gd). For *Ln* = Eu and Gd, the best refinements were achieved by including all reflections from both twin lattices. Reflections were scaled based on the degree of overlap with the complementary lattice. Eight separate scale factors were used. Based on these refined scale factors, the major twin volumes were calculated to be Pr: 0.689(2); Eu: 0.72(1); Gd: 0.53(1). For *Ln* = Tb, the major component dominated to such an extent (90%) that the best refinement was achieved by wholly neglecting the minor twin lattice. Structural refinements on the Sm analogue did not yield satisfactory statistics. The crystal data and co-ordinates reported in Tables 1 and 2 correspond to the data obtained from crystals twinned by two-fold rotation for *Ln* = Pr, Eu and Gd.

Initial structure refinements with the atomic co-ordinates resulted in unacceptably large electron density peaks in all cases (largest being $>18\,e^-/Å^3$ for *Ln* = Gd) except for *Ln* = Pr, indicating disorder in the crystal structure. For crystals twinned by mirror plane, (*Ln* = Eu, Gd), the disorder corresponded to $\frac{1}{2},0,0$, shift of atom *Ln*(3), while for crystals twinned by two fold rotation (*Ln* = Pr, Eu, Gd), the disorder corresponded to a $0,0,\frac{1}{2}$, shift of atoms *Ln*(3), Ru(1) and O(3)/O(4) similar to the disorder/defect model employed in the refinement of $Y_5Re_2O_{12}$. [8] Final refined occupancies for the major/minor disorder fractions were observed to be: Eu, 0.956(4)/0.044(4); Gd, 0.951(6)/0.049(6); Tb, 0.977(2)/0.0233(2) (all restrained to sum to unity). For *Ln* = Eu, only the Eu atoms were refined anisotropically. For *Ln* = Gd, all atoms except O(4) were refined anisotropically. For *Ln* = Pr and Tb, all atoms were refined anisotropically. Atoms of the minor disorder fraction were refined isotropically in all cases, and the displacement parameters of O(3A) and O(4A) were fixed at values near the average of the refined U_{iso} for the other minor component atoms and were not refined. For *Ln* = Tb, an additional Tb(3) disorder component (Tb(3B)) shifted by $0,\frac{1}{2},\frac{1}{2}$ was necessary to account for the extra electron density. The occupancy of Tb(3) was then adjusted manually to achieve the nominal stoichiometry.

The instabilities in thermal parameters and relatively large residual electron density extremes for oxides with *Ln* = Sm, Eu and Gd, reflect the reduced precision arising from the combined twin/disorder model necessary for convergence of structure refinements. However, no disorder was observed in the case of $Pr_5Ru_2O_{12}$ and the structural model was found to be similar to that of $Tm_5Re_2O_{12}$ [23]. The presence of twinning in these oxides was further confirmed by HRTEM studies (Fig. 2a–c). Fig. 2a and b shows representative TEM images at low magnification of $Gd_5Ru_2O_{12}$ (a) and $Nd_5Ru_2O_{12}$ (b), depicting the twin fractions. While the images depict the major twin component, the accolades in the images indicate the small areas showing the minor twin component.

The single crystal X-ray structure of $Ln_5Ru_2O_{12}$ (*Ln* = Pr, Nd–Tb) (Fig. 3) is isotypic with that of $Ln_5M_2O_{12}$ (*M* = Mo, Re) [7–9,18–20]. The dominant feature of the structure is the presence of one-dimensional chains consisting of edge-sharing RuO_6 octahedra along the *b* axis, separated by a two dimensional LnO_x polyhedral framework. The RuO_6 octahedral chains are isolated from each other. Each pair of edge shared RuO_6 octahedra is separated alternately by *Ln*(3) and the disordered component of *Ln*(3) atom (*Ln*(3A)). This feature is observed as stacking faults in

the HRTEM images. An enlarged image (focus and thickness values of 20 and 25 nm, respectively) of such a stacking fault (central in the image) is shown in Fig. 2c. The white dots correspond to the projections of the cation columns while the black dots correspond to those of the oxygen columns in the crystal structure. The arrows indicate the Gd–O and Ru–O layers shifted by a magnitude of $c/2$, relative to each other.

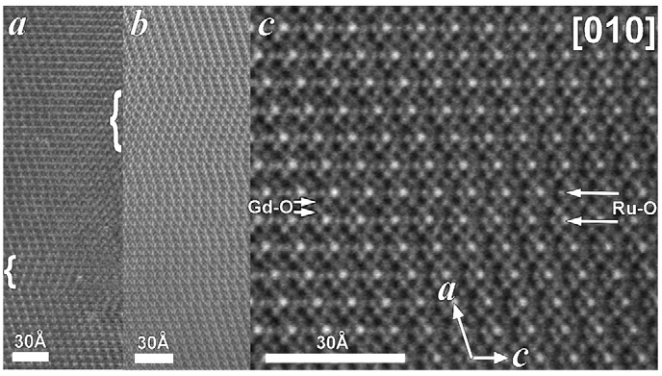

Fig. 2. TEM images of: (a) $Gd_5Ru_2O_{12}$, (b) $Nd_5Ru_2O_{12}$, and (c) an atomic resolution picture of a stacking fault in $Gd_5Ru_2O_{12}$.

The RuO_6 octahedral chains (Fig. 4) consist of alternating short (2.800(1)–2.824(1) Å) and long (3.083(1)–3.145(1) Å) Ru–Ru distances, also observed in other phases with this structure type. The short *M*–*M* (Ru–Ru) distances in $Ln_5Ru_2O_{12}$ are slightly longer than the *M*–*M* (Mo–Mo) distances found in $Y_5Mo_2O_{12}$ [9] (2.446 (1) Å) and the long distances are slightly shorter than those reported for Ln_5MO_{12} (M = Mo, Re) type [7–9,18–22] (3.748(1) Å) for $Y_5Re_2O_{12}$ [8]. The ruthenium atoms in $Ln_5Ru_2O_{12}$ (Ln = Pr, Sm–Tb) have an average oxidation state of +4.5 and the Ru–O distances range between 1.927(7) Å and 2.046(3) Å, thus falling into the known range of Ru–O bond length observed for other $Ru^{+4.5}$ systems [23]. The *Ln*(1) and *Ln*(2) atoms are seven-fold coordinated and form mono-capped trigonal prisms (Fig. 3) while *Ln*(3) atoms are octahedrally coordinated and are involved in the connectivity of the edge shared RuO_6 chains along the *c*-axis, which form slabs in the *bc* plane (Fig. 3). The *Ln*(1)O_7 and *Ln*(2)O_7 polyhedra connect these slabs to form the condensed structure.

The occurrence of alternating long and short *M*–*M* distances in similar Ln_2MO_{12} (M = Mo, Re) oxides has been explained to be due to *M*–*M* bond formation [8,9] with the unpaired electron localized within the M_2 dimer. Based on the crystallographic data, it is reasonable to suspect that this is true also in case of $Ln_5Ru_2O_{12}$ (Ln = Pr, Sm–Tb) oxides. Magnetic susceptibility data *vide infra* is however inconclusive.

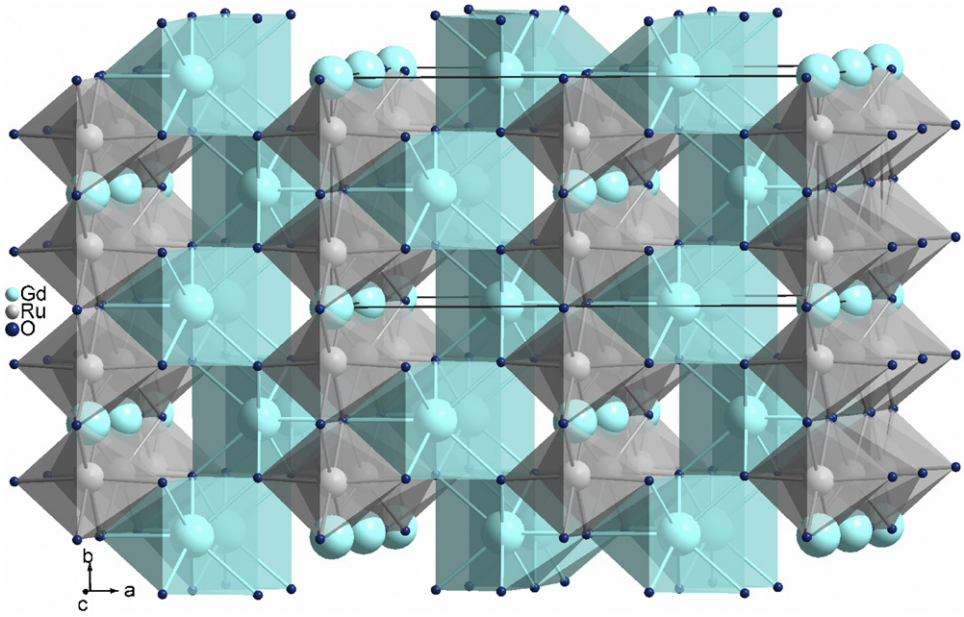

Fig. 3. Crystal structure of $Ln_5Ru_2O_{12}$ (Ln = Pr, Nd, Sm–Tb).

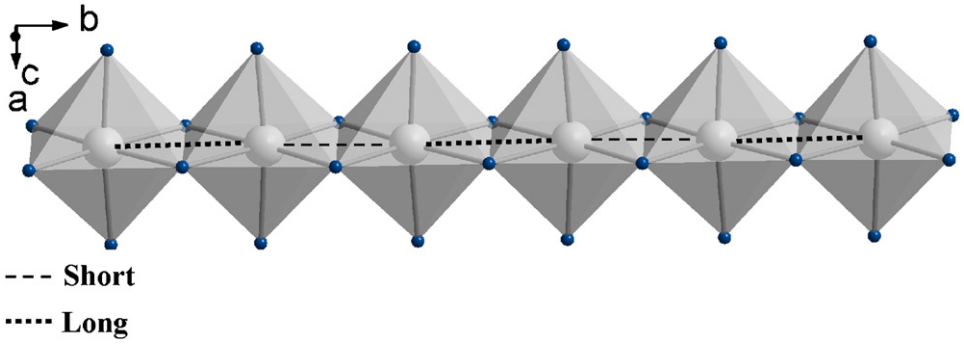

Fig. 4. Infinite chains of edge shared RuO_6 octahedra illustrating the alternate short and long Ru to Ru bond distances in $Ln_5Ru_2O_{12}$ (Ln = Pr, Nd, Sm–Tb). The dotted lines represent the long bonds while the dashed lines represent the short bonds.

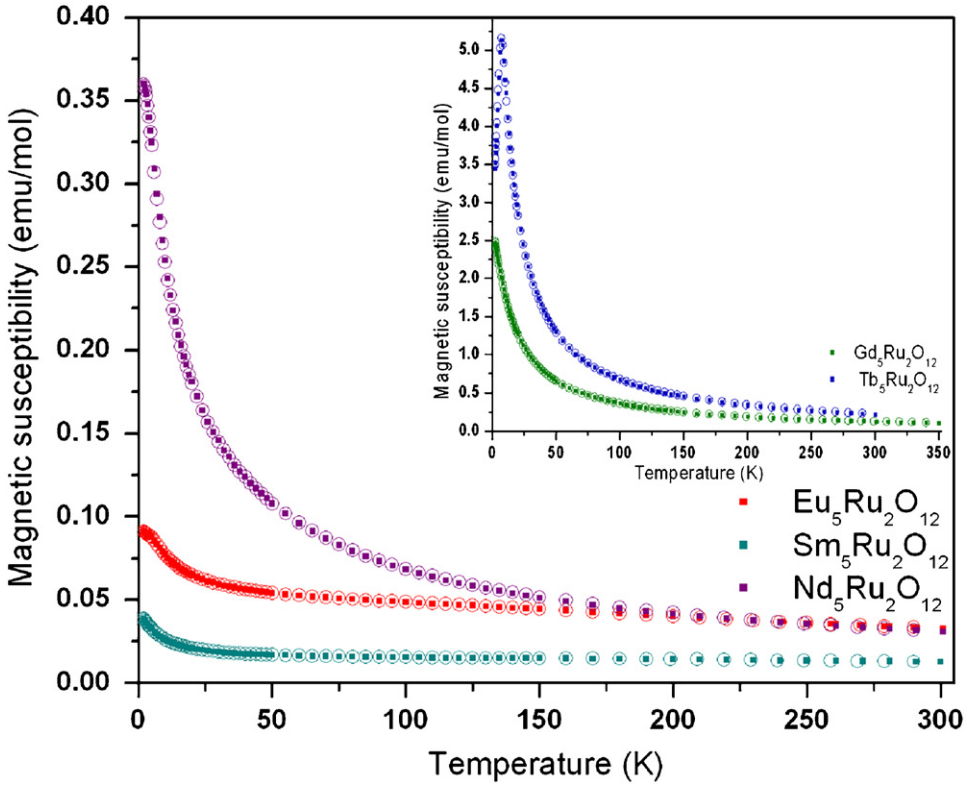

Fig. 5. Magnetic susceptibilities of $Ln_5Ru_2O_{12}$ (Ln = Eu, Nd, Sm) in an applied field of 10 kG. The inset shows the susceptibilities of $Gd_5Ru_2O_{12}$ and $Tb_5Ru_2O_{12}$ in applied fields of 10 and 1 kG, respectively. The open circles indicate zero-field-cooled data while filled squares represent field-cooled data.

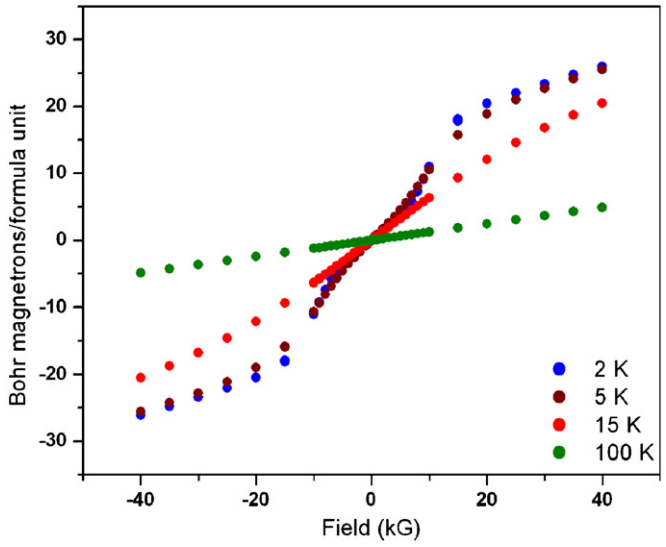

Fig. 6. Field dependence of the magnetization of $Tb_5Ru_2O_{12}$ collected at 100, 15, 5, and 2 K.

3.2. Magnetism

3.2.1. $Ln_5Ru_2O_{12}$ (Ln = Nd, Sm–Tb)

The temperature dependence of the magnetic susceptibilities of $Ln_5Ru_2O_{12}$ (Ln = Nd, Sm and Eu,) measured in an applied field of 10 kG are shown in Fig. 5. The inset to Fig. 5 shows the susceptibilities of $Gd_5Ru_2O_{12}$ and $Tb_5Ru_2O_{12}$ in applied fields of 10 and 1 kG, respectively. The magnetic susceptibility data of Sm and Eu exhibit no long-range order down to the lowest measured temperature (2 K), and exhibit significant deviation from Curie–Weiss type behavior, consistent with susceptibility measurements on other oxides of samarium and europium [24,25]. However, the (Ln = Nd, Gd, Tb) analogues of $Ln_5Ru_2O_{12}$ show Curie–Weiss type paramagnetic behavior with μ_{eff} values of = 9.49, 18.1 and 23.5 μ_B, and $\theta = -63$, -12, and -2 K, respectively, which are in good agreement with the theoretical μ_{eff} values of 9.41, 19.0 and 22.3 μ_B. $Tb_5Ru_2O_{12}$ exhibits antiferromagnetic order at 7 K. The values of μ_{eff} for all the oxides correspond to the contribution from both the rare earth (Ln^{3+}) and ruthenium (Ru^{4+} and Ru^{5+}) ions. The field dependence of the magnetization of $Tb_5Ru_2O_{12}$ recorded at 100, 15, 5, and 2 K is shown in Fig. 6. At 100 K, the plot is linear indicating paramagnetic behavior. At temperatures below the AF ordering temperature, field dependence is observed; however, the magnetization does not appear to reach saturation at the highest measured field of 40 kG.

4. Conclusion

Oxides, $Ln_5Ru_2O_{12}$ (Ln = Pr, Nd, Sm–Tb) were prepared as single crystals from fluxes of either NaOH or KOH in sealed silver tubes. These phases represent the first examples of this structure type containing ruthenium as the transition metal. The average oxidation state of ruthenium in these oxides is +4.5. The crystals of all the phases were observed to be twinned as confirmed by TEM studies. The crystal structure is isotypic with the defect/disorder model of $Ln_5Re_2O_{12}$ and consists of one-dimensional chains of edge shared RuO_6 octahedra separated by a two dimensional LnO_x polyhedral framework. TEM studies are in agreement with the simulated structural model from single crystal X-ray diffraction data. Magnetic measurements indicate paramagnetic and antiferromagnetic behavior for Ln = Nd, Sm–Gd and Ln = Tb, respectively.

Supplemental information

Further details of the crystal structure investigations can be obtained from the Fachinformationszentrum Karlsruhe, 76344 Eggenstein-Leopoldshafen, Germany (fax: (49) 7247-808-666; E-mail: crystdata@fiz-karlsruhe.de) on quoting the depository numbers CSD–419957-419960.

Acknowledgments

Financial support from the National Science Foundation through Grants DMR:0450103 and DMR:0804209 is gratefully acknowledged.

Appendix A. Supplementary material

Supplementary data associated with this article can be found in the online version at doi:10.1016/j.jssc.2009.02.013.

References

[1] M. Hase, I. Terasaki, K. Uchinokara, Phys. Rev. Lett. 70 (1993) 3651–3654.
[2] C. Kim, A.Y. Matsuara, Z.X. Shen, N. Motoyama, H. Eisaki, S. Uchida, T. Tohyama, S. Maekawa, Phys. Rev. Lett. 77 (1996) 4054–4057.
[3] R. Lam, F. Wiss, J.E. Greedan, J. Solid State Chem. 167 (2002) 182–187.
[4] H. Prevost-Czeskleba, J. Less Common Metals 127 (1987) 117–124.
[5] J.E. Greedan, N.P. Raju, A. Wegner, P. Gougeon, J. Padiou, J. Solid State Chem. 129 (1997) 320–327.
[6] J.F. Vente, D.J.W. Ijdo, Mater. Res. Bull. 21 (1986) 1103–1106.
[7] W. Jeitschko, D.H. Heumannskämper, U.C. Rodewald, M.S. Schriewer-Pöttgen, Z. Anorg. Allg. Chem. 626 (2000) 80–88.
[8] L. Chi, J.F. Britten, J.E. Greedan, J. Solid State Chem. 172 (2003) 451–457.
[9] C.C. Torardi, C. Fecketter, W.H. McCarrol, F.J. DiSalvo, J. Solid State Chem. 60 (1985) 332–342.
[10] J. Darriet, F. Grasset, P.D. Battle, Mater. Res. Bull. 32 (1997) 139–150.
[11] P.D. Battle, C.P. Grey, M. Hervieu, C. Martin, C.A. Moore, Y. Paik, J. Solid State Chem. 175 (2003) 20–26.
[12] M.J. Davis, M.D. Smith, K.E. Stitzer, H.-C. zur Loye, J. Alloys Compd. 351 (2003) 95–100.
[13] W.R. Gemmill, M.D. Smith, H.-C. zur Loye, Inorg. Chem. 46 (2007) 2132–2138.
[14] SADABS Version 2.10, Bruker Analytical X-ray Systems, Madison, Wisconsin, USA, 2003.
[15] G.M. Sheldrick, SHELXS97, Program for Crystal Structure Solution, University of Gottingen, Germany, 1997.
[16] V. Petricek, M. Ducek, JANA2000, Structure Determination Software Programs, Institute of Physics: Praha, Czech Republic, 2000.
[17] G.M. Sheldrick, SHELXS97, Program for Crystal Structure Solution, University of Gottingen, Germany, 1997.
[18] GEMINI Version 1.02, Bruker Analytical X-ray Systems, Madison, Wisconsin, USA, 1999.
[19] A.L. Spek, PLATON, A Multipurpose Crystallographic Tool, Utrecht University, Utrecht, The Netherlands, 1998.
[20] A.D. Savel'eva, M.B. Varfolomeev, V.V. Fomichev, K.I. Petrov, Z. Neorg. Khim. 22 (1977) 2994–2997.
[21] G. Baud, J.-P. Besse, M. Capestan, R. Chevalier, Ann. Chim. Fr. 7 (1982) 615–621.
[22] G. Baud, J.-P. Besse, R. Chevalier, Mater. Chem. Phys. 8 (1983) 93–99.
[23] K.E. Stitzer, M.D. Smith, W.R. Gemmill, H.-C. zur Loye, J. Am. Chem. Soc 124 (2002) 13877–13885.
[24] K. Koteswara Rao, M. Vithal, D. Ravinder, J. Magn. Magn. Mater. 253 (2002) 65–71.
[25] L. Thompson, J. Legendziwicz, J. Cybinska, L. Pan, W. Brennessel, J. Alloys Compd. 341 (2002) 312–322.